

# Raman light scattering study and microstructural analysis of epitaxial films of the electron-doped superconductor $\text{La}_{2-x}\text{Ce}_x\text{CuO}_4$

M. Rahlenbeck<sup>1</sup>, M. Wagenknecht<sup>2,3</sup>, A. Tsukada<sup>3</sup>, D. Koelle<sup>2</sup>, R. Kleiner<sup>2</sup>, B. Keimer<sup>1</sup>, and C. Ulrich<sup>1,4,5</sup>

<sup>1</sup>*Max-Planck-Institut für Festkörperforschung, Heisenbergstraße 1, D-70569 Stuttgart, Germany*

<sup>2</sup>*Physikalisches Institut - Experimentalphysik II, Universität Tübingen,*

*Auf der Morgenstelle 14, D-72076 Tübingen, Germany*

<sup>3</sup>*NTT Basic Research Laboratories, NTT Corporation,*

*3-1 Morinosato-Wakamiya, Atsugi, Kanagawa 243-0198, Japan*

<sup>4</sup>*University of New South Wales, School of Physics, 2052 Sydney, New South Wales, Australia and*

<sup>5</sup>*The Bragg Institute, Australian Nuclear Science and Technology Organization, Lucas Heights, NSW 2234, Australia*

(Dated: June 22, 2021)

We present a detailed temperature-dependent Raman light scattering study of optical phonons in molecular-beam-epitaxy-grown films of the electron-doped superconductor  $\text{La}_{2-x}\text{Ce}_x\text{CuO}_4$  close to optimal doping ( $x \sim 0.08$ ,  $T_c = 29$  K and  $x \sim 0.1$ ,  $T_c = 27$  K). The main focus of this work is a detailed characterization and microstructural analysis of the films. Based on micro-Raman spectroscopy in combination with x-ray diffraction, energy-dispersive x-ray analysis, and scanning electron microscopy, some of the observed phonon modes can be attributed to micron-sized inclusions of  $\text{Cu}_2\text{O}$ . In the slightly underdoped film ( $x \sim 0.08$ ), both the  $\text{Cu}_2\text{O}$  modes and others that can be assigned to the  $\text{La}_{2-x}\text{Ce}_x\text{CuO}_4$  matrix show pronounced softening and narrowing upon cooling below  $T \sim T_c$ . Based on control measurements on commercial  $\text{Cu}_2\text{O}$  powders and on a comparison to prior Raman scattering studies of other high-temperature superconductors, we speculate that proximity effects at  $\text{La}_{2-x}\text{Ce}_x\text{CuO}_4/\text{Cu}_2\text{O}$  interfaces may be responsible for these anomalies. Experiments on the slightly overdoped  $\text{La}_{2-x}\text{Ce}_x\text{CuO}_4$  film ( $x \sim 0.1$ ) did not reveal comparable phonon anomalies.

PACS numbers:

Electron-doped high-temperature superconductors exhibit a substantially lower maximum transition temperature and a narrower doping range of superconductivity than their hole-doped counterparts. The origin of this asymmetry of the phase diagram is still incompletely understood, in part due to the complex materials physics of the electron-doped cuprates. It has been demonstrated, for instance, that the elaborate annealing procedure required to stabilize superconductivity in bulk single crystals of  $\text{Nd}_{2-x}\text{Ce}_x\text{CuO}_4$  (NCCO), one of the most widely studied electron-doped cuprates, generates a small amount of an epitaxially intergrown impurity phase that profoundly affects the magnetic properties.[1] Similar observations have been reported for some epitaxial thin films of  $\text{Pr}_{2-x}\text{Ce}_x\text{CuO}_4$  (PCCO) grown by pulsed-laser deposition.[2] The pervasiveness of such inclusions and their influence on various physical properties is only beginning to be explored, but the wide variation of the transport characteristics of thin films of nominally identical composition [3] suggests that they may be quite common.

Since Raman scattering is both a powerful spectroscopic probe of superconductivity in the cuprates and an excellent diagnostic tool for impurity phases, we have carried out a high-resolution Raman scattering study of molecular beam epitaxy (MBE)-grown films of  $\text{La}_{2-x}\text{Ce}_x\text{CuO}_4$  (LCCO), the compound that exhibits both the highest critical temperature and the widest doping range for superconductivity among all electron-doped cuprates.[4–6] LCCO crystallizes in the so-called  $T'$ -structure, which does not include apical oxygen ions, in contrast to the  $T$ -structure found in hole-doped mem-

bers of the  $\text{Ln}_2\text{CuO}_4$  family. The stability of the  $T'$ -structure depends on the radius of the lanthanide ( $\text{Ln}$ ) ions.[4] For  $\text{Ln} = \text{La}$ , the  $T'$ -structure is unstable in bulk form, but can be stabilized by epitaxial growth on  $\text{SrTiO}_3$  substrates.[4] Depending on the growth conditions, LCCO can also crystallize in the  $T$ -structure, but superconductivity is observed only in the  $T'$ -structure.[7, 8] The superconducting state is stable over a wider doping range ( $0.05 \leq x \leq 0.22$ ) than in other electron-doped compounds such as NCCO, and the maximum transition temperature ( $T_c \sim 30$  K) is found at a lower doping level ( $x = 0.09$ , compared to 0.15 for NCCO).[6, 9]

In the hole-doped cuprates, numerous Raman scattering experiments have elucidated the magnitude, anisotropy, and doping dependence of the superconducting energy gap,  $\Delta$ , either directly via electronic Raman scattering [10] or indirectly via phonon anomalies induced by the electron-phonon interaction.[11, 12] In electron-doped superconductors, electronic Raman scattering [13, 14] has also yielded valuable information about the magnitude and anisotropy of  $\Delta$ , but superconductivity-induced phonon anomalies have thus far not been reported. Since electronic Raman scattering is difficult in films, we have used the latter method in an attempt to gain insight into the energy gap of LCCO. We indeed observe phonon anomalies at temperatures close to the superconducting transition temperature  $T_c$ , but find that micron-sized  $\text{Cu}_2\text{O}$  inclusions present in all samples complicate their interpretation.

The Raman scattering experiments were performed on two 900 nm thick LCCO films that had been the

basis of prior transport experiments.[15] The films had been deposited epitaxially on [001]-oriented SrTiO<sub>3</sub> substrates, yielding *c*-axis oriented films, in two independent fabrication runs using MBE from pure metal sources, as described elsewhere.[4] After growth, they were annealed in vacuum at 578°C and 559°C for 100 and 90 minutes, respectively, in order to remove residual apical oxygen ions.[16] The Ce concentrations were adjusted to  $x \sim 0.08$  (corresponding to electron concentrations slightly less than optimum doping) and  $x \sim 0.1$  (slightly overdoped) by exact control of the gas flux rates and use of inductively coupled plasma - atomic emission spectroscopy (ICP-AES).[16, 17] Electrical resistivity measurements revealed  $T_c \sim 29$  K and 27 K, respectively. The widths of the resistivity transitions at  $T_c$  were below 1 K for both films. For comparison, we used one platelet-like Cu<sub>2</sub>O single crystal with *c*-axis perpendicular to the surface, and two commercial Cu<sub>2</sub>O powder samples. Powder (I) had a purity of 99.9% with maximal impurity content of 0.006% Fe, 0.004% Si, 0.003% Pb, 0.002% Mn, and 3 ppm Sb (as indicated by the supplier). Powder (II) had a purity of 99.5%, and the supplier did not provide information about the nature of the impurities.

For the Raman measurements we used two different setups. In order to maximize the spectral resolution we used a “macro” setup, where the samples were mounted in a vertical helium-flow cryostat. The spectra were taken in quasi-backscattering geometry using the linearly polarized 514.5 nm and 488.0 nm lines of an Ar<sup>+</sup>/Kr<sup>+</sup> mixed-gas laser for excitation. The laser beam was focused on a  $\sim 100$   $\mu\text{m}$  spot on the sample surface with an incident power of less than 10 mW, in order to avoid sample heating. The scattered light was analyzed by a DILOR XY triple grating spectrometer using a nitrogen-cooled charge-coupled-device (CCD) camera. For higher spatial resolution we used a “micro” setup, where the samples were mounted on the cold finger of a horizontal helium-flow cryostat. The spectra were taken in backscattering geometry using the linearly polarized 532.0 nm line of a frequency doubled Nd:YAG laser for excitation. The laser beam was focused through a 50 $\times$  (10 $\times$ ) microscope objective to a  $\sim 3$   $\mu\text{m}$  ( $\sim 10$   $\mu\text{m}$ ) diameter spot on the sample surface, with an incident laser power of less than 1 mW. The scattered light was analyzed by a JobinYvon LabRam single grating spectrometer equipped with a notch filter and a Peltier-cooled CCD camera. For each Raman spectrum an additional calibration spectrum of a nearby argon or neon line was measured in order to accurately determine the frequency and linewidth of the different phonons. For data analysis, all phonon peaks were fitted to Voigt profiles, which result from a convolution of the Lorentzian phonon lineshape with the Gaussian shaped instrumental resolution ( $\sim 4$   $\text{cm}^{-1}$  full width at half maximum (FWHM) for the macro setup).

Figure 1 shows the Raman spectrum of the slightly underdoped LCCO film at temperature  $T = 30$  K in the *z*(xx)*z* polarization configuration. Here, we use the Porto

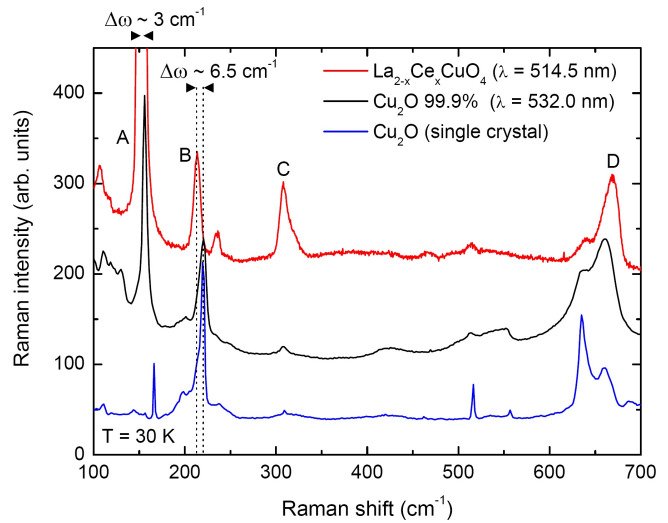


FIG. 1: Raman spectra at 30 K of (top) the slightly underdoped LCCO film ( $T_c \sim 29$  K) in *z*(xx)*z* polarization configuration for 514.5 nm laser excitation, (middle) the Cu<sub>2</sub>O powder sample (99.9 %), and (bottom) the Cu<sub>2</sub>O single crystal each for 532.0 nm laser excitation. (Cu<sub>2</sub>O spectra scaled for clarity.)

notation  $l(ij)m$ , where  $l$  and  $m$  denote the direction of incident and scattered light and  $(ij)$  their polarization, respectively. Both the slightly underdoped and the slightly overdoped LCCO films show comparable Raman spectra. We detect four main modes at  $153.5$   $\text{cm}^{-1}$  (mode A),  $213.5$   $\text{cm}^{-1}$  (mode B),  $308.5$   $\text{cm}^{-1}$  (mode C), and a double mode at  $\sim 640$ - $670$   $\text{cm}^{-1}$  (mode D). A mode at  $\sim 429$   $\text{cm}^{-1}$ , which would correspond to an apical oxygen vibration in the *T*-structure of La<sub>2</sub>CuO<sub>4</sub> (Ref. [11]), is not observed, indicating the absence of apical oxygen residuals. A group theoretical analysis of the phonon modes of the *T'*-structure (tetragonal space group  $I4/mmm$  ( $D_{4h}^{17}$ )) [18] yields  $A_{1g} + B_{1g} + 2E_g$  Raman-active modes. To our knowledge, Raman data on *T'*-LCCO have not yet been reported. We therefore use data on related *T'*-lanthanide cuprates such as NCCO for comparison [11, 19, 20]. The energies of modes B and C are close to, but somewhat lower than those of the  $A_{1g}$  and  $B_{1g}$  vibrations, respectively, of the Nd and out-of-plane oxygen atoms in *T'*-NCCO.[20] A downward shift of the LCCO modes with respect to NCCO would be in line with a continuous frequency evolution previously observed in the series of lanthanide cuprates [20].

The assignment of modes A and D is more difficult, because Raman spectra of other cuprates with the *T'*-structure do not exhibit modes with similar energies. We have therefore investigated possible contamination by impurity phases, including Cu<sub>2</sub>O which has been previously observed as a contaminant in NCCO.[18] Figure 1 shows a comparison to reference spectra of compressed Cu<sub>2</sub>O powder sample I (99.9 % purity) and the Cu<sub>2</sub>O single crystal for 532.0 nm laser excitation. Based on this comparison and on earlier data on Cu<sub>2</sub>O [21, 22],

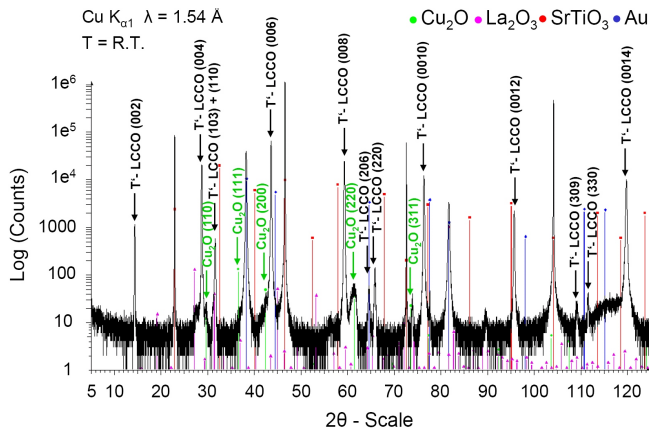


FIG. 2: X-ray  $\Theta$ - $2\Theta$ -scan of the slightly underdoped LCCO film at room temperature (Cu  $K_{\alpha 1}$  with  $\lambda = 1.54 \text{ \AA}$ ). The Bragg reflections of  $\text{SrTiO}_3$  and gold are due to the substrate and gold contacts on top of the film.

modes A and D can be identified with the infrared-allowed  $\Gamma_{15}^{(1)}$  and  $\Gamma_{15}^{(2)}$  modes of  $\text{Cu}_2\text{O}$ . [23] Due to resonance effects, these modes can become Raman-active with high intensity. [24, 25] The much stronger intensity of the  $\Gamma_{15}^{(1)}$  mode in the  $\text{Cu}_2\text{O}$  powder compared to the  $\text{Cu}_2\text{O}$  single crystal can be attributed to powder averaging over all possible polarization geometries. Mode A in the LCCO films also shows high intensity, suggesting an isotropic orientation of the  $\text{Cu}_2\text{O}$  impurity phase. The shift of  $\sim 3 \text{ cm}^{-1}$  of mode A with respect to the  $\Gamma_{15}^{(1)}$  mode of  $\text{Cu}_2\text{O}$  may be a consequence of stress imposed by the LCCO matrix. Note that modes with energies roughly comparable to those of modes B and C are also present in the  $\text{Cu}_2\text{O}$  reference spectra, but the former mode is shifted by  $\sim 6.5 \text{ cm}^{-1}$  with respect to mode B, and the latter mode is extremely weak. We will show below that these modes likely originate from LCCO.

In order to directly characterize the chemical composition of the LCCO films, we used high-intensity x-ray diffraction (XRD). Figure 2 shows a  $\Theta$ - $2\Theta$  scan of the slightly underdoped LCCO film at room temperature, plotted on a logarithmic intensity scale. Based on a comparison with the calculated Bragg angles for the  $T'$ -structure [4], we clearly identify the expected [001]-oriented  $T'$ -structure as the main phase. Additional XRD pole figure measurements (not shown here) also reveal the Bragg peaks (103) and (110). This indicates two  $T'$ -LCCO minority phases with different growth directions, which are stabilized by a well-known, accidental match between the in-plane and out-of-plane lattice parameters ( $c/a \approx 3$ ). We find no indication for the presence of any  $T$ -structure inclusions. The XRD measurements also confirm the presence of a  $\text{Cu}_2\text{O}$  impurity phase, as well as a trace amount of  $\text{La}_2\text{O}_3$  (Fig. 2). The intensities of the main  $\text{Cu}_2\text{O}$  Bragg reflections are about four orders of magnitude below those of LCCO, but their ratios indicate random orientation of the  $\text{Cu}_2\text{O}$  crystal-

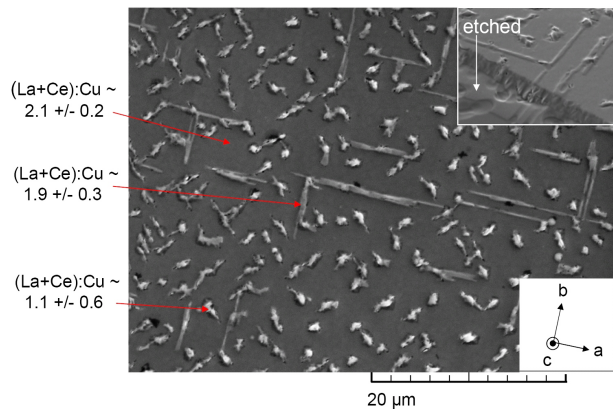


FIG. 3: SEM image of the slightly underdoped LCCO film. The upper inset shows a partly etched surface area.

lites, in contrast to the epitaxially oriented LCCO matrix. Taking powder averaging of the  $\text{Cu}_2\text{O}$  Bragg reflections into account, the XRD data imply that the volume fraction of  $\text{Cu}_2\text{O}$  is only about an order of magnitude below the one of LCCO.

The microstructure and the local variation of the chemical composition of the LCCO films were further analyzed by scanning electron microscopy (SEM) and energy dispersive x-ray (EDX) analysis. The microstructure of both LCCO films appeared comparable. Figure 3 shows a SEM image of the slightly underdoped LCCO film. About 18% of the surface area is uniformly flecked with particles of  $\sim 3 \mu\text{m}$  diameter. While the surface background exhibits the composition ratio  $(\text{La}+\text{Ce}):\text{Cu} \sim 2.1 \pm 0.2$  characteristic of  $T'$ -LCCO, the particles were found to be centers of strongly enhanced Cu content, with the statistically averaged ratio  $(\text{La}+\text{Ce}):\text{Cu} \sim 1.1 \pm 0.6$ . They are thus good candidates for the  $\text{Cu}_2\text{O}$  impurity phase. The high and uniform surface coverage with particles supports the picture of an isotropically oriented  $\text{Cu}_2\text{O}$  impurity phase of  $\gtrsim 10\%$  in the LCCO films. In addition, we observed line structures oriented along the  $ab$  crystal axes, which exhibit a slightly enhanced Cu content. These structures may originate from structural defects or from the  $T'$ -LCCO minority phases. In the inset of figure 3 we show a surface area of the slightly underdoped LCCO film, which was partly etched by Ar ion bombardment. We find that both the particles and the line structures reach deeply into the film, suggesting their formation during the crystal growth. The concentrations of impurity atoms beyond the constituent elements of LCCO were below the EDX detection limit.

In order to relate the Raman spectra of Fig. 1 to the microscopic observations of Fig. 3, we employed the micro-Raman setup. Figure 4a shows a line scan of the intensity of mode A in the slightly underdoped LCCO film. The intensity varies strongly on a length scale of  $\sim 3 \mu\text{m}$ , which is comparable to the size of the particles in Fig. 3. This underscores the assignment of this mode to the  $\text{Cu}_2\text{O}$  impurity phase. The intensities of

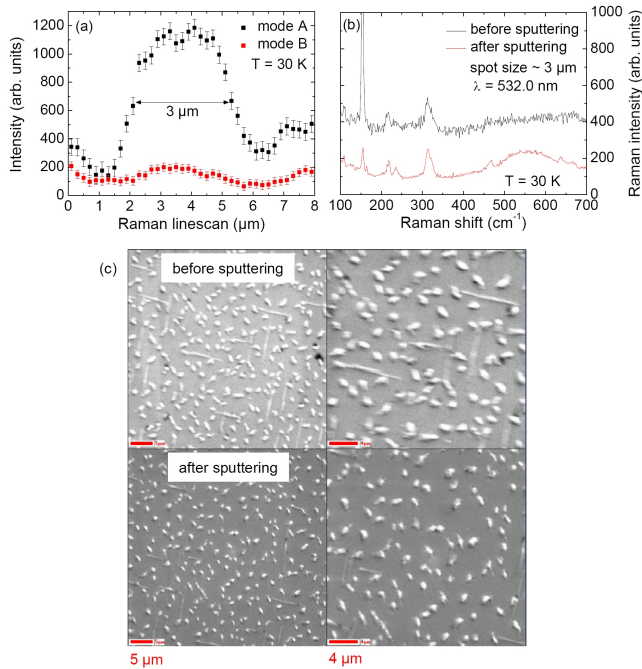


FIG. 4: (a) Line scan of the intensities of modes A and B of the underdoped LCCO film taken in the micro-Raman setup with  $50\times$  microscope objective and  $\lambda = 532.0$  nm, (b) Raman spectra at  $T = 30$  K before and after sputtering of  $\sim 250$  nm, and (c) SEM images before and after sputtering.

modes B and C, on the other hand, depend only weakly on the measuring position (Fig. 4a), supporting the conclusion that they do not originate from  $\text{Cu}_2\text{O}$ , but from the  $T'$ -LCCO host material. We used argon ion sputtering under vacuum in an attempt to remove the  $\text{Cu}_2\text{O}$  particles. A comparison of SEM images of the surface before and after removal of  $\sim 250$  nm (Fig. 4c) confirms that the particles are stuck deeply inside the LCCO matrix. While it is thus not possible to remove the particles, sputtering still reduces both the volume fraction of  $\text{Cu}_2\text{O}$  and the intensity of mode A (Fig. 4b). Modes B and C, on the other hand, are nearly unaffected by sputtering.

Having obtained a thorough understanding of the microstructure and phase composition of the LCCO films, we now focus on anomalies in the temperature dependence of the different optical modes at the superconducting transition temperature  $T_c$ . Figure 5 shows the Raman spectra of the slightly underdoped LCCO film from 10 K to 300 K in  $z(xx)z$  polarization for 514.5 nm laser excitation. The integrated intensities of modes A and D show a strong temperature dependence with a significant increase below  $T \sim 150$  K. A similar activation was also observed in the  $\text{Cu}_2\text{O}$  reference samples (not shown here), again confirming their common origin. In contrast, the intensities of modes B and C exhibit a much weaker temperature dependence. Figure 6a shows the temperature dependence of the frequency and FWHM of mode A. The solid lines are the result of fits to the data above  $T_c$ , using an expression based on anharmonic phonon-

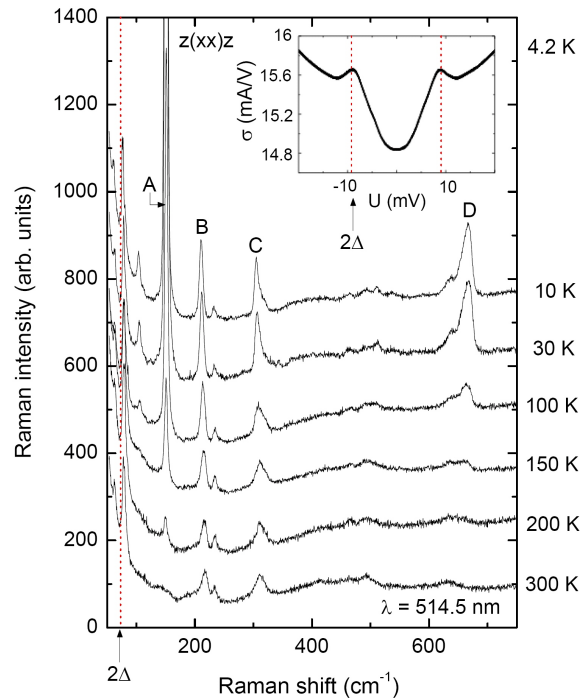


FIG. 5: Raman spectra of the slightly underdoped LCCO film at temperatures  $10 \text{ K} \leq T \leq 300 \text{ K}$  in  $z(xx)z$  polarization configuration for 514.5 nm laser excitation.  $2\Delta \sim 9$  meV denotes the energy of the superconducting gap. The inset shows the corresponding quasiparticle conductance at 4.2 K.

phonon interactions [26, 27]. For simplicity we assumed a symmetric decay into two product modes, which leads to the following expressions for the phonon frequency  $\omega_{ph}$  and FWHM  $\Gamma_{ph}$ :

$$\omega_{ph}(T) = -A \left( 1 + \frac{2a}{\exp(\hbar\omega_0/2k_B T) - 1} \right) + \omega_0,$$

$$\Gamma_{ph}(T) = \Gamma_a \left( 1 + \frac{2a}{\exp(\hbar\omega_0/2k_B T) - 1} \right) + \Gamma_b,$$

where  $A$  and  $\Gamma_a$  are positive constants and  $a$  corrects for terms arising from nonsymmetric phonon decay processes.  $\Gamma_b$  represents the temperature-independent part of  $\Gamma_{ph}$ .

While mode A follows nearly perfectly the expression for anharmonic decay in the normal state, we observe significant deviations from this behavior below  $T \sim T_c$ . The frequency softens by  $\sim 0.7 \text{ cm}^{-1}$  upon cooling below  $T_c$ , and the temperature dependence of the linewidth exhibits a change in slope in the same temperature range, which corresponds to a narrowing of  $\sim 0.5 \text{ cm}^{-1}$ . The deviations from the anharmonic behavior are illustrated by the shaded areas in figure 6a. In contrast to mode A, the temperature dependence of the parameters characterizing modes B and C differs substantially from the standard anharmonic behavior (Figs. 6b and c). In particular, their frequencies increase continuously with increasing  $T$ , opposite to the behavior expected from an-

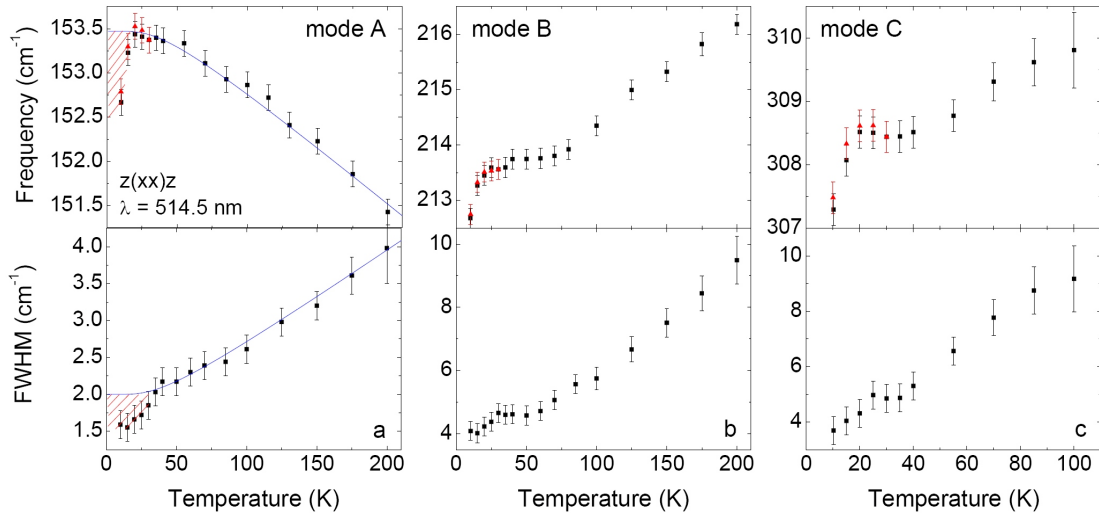


FIG. 6: Temperature dependence of the frequency and FWHM of modes A, B, and C in the underdoped LCCO film (see Fig. 1). The triangular points represent a second independent data set at low temperatures. The solid lines are the result of fits to the data points above  $T_c$  according to the theory of anharmonic phonon decay [26, 27] (see text for details). The shaded areas indicate deviations from the anharmonic temperature dependence below  $\sim T_c$ .

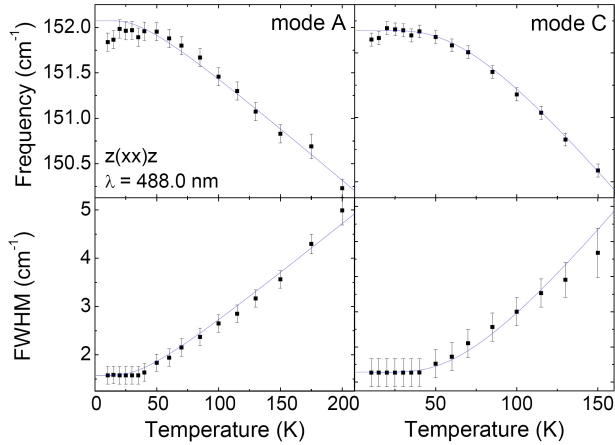


FIG. 7: Temperature dependence of the frequency and FWHM of modes A and C in the slightly overdoped LCCO film ( $T_c \sim 27$  K). The 487.986 nm laser line was used for excitation. For solid lines see caption of figure 6.

harmonicity. Below  $T_c$ , however, they exhibit softening and narrowing of the same magnitude as the one observed for mode A. Remarkably, both the anomalous normal-state behavior of mode C and the renormalization of the phonon frequencies below  $T_c$  are absent in the slightly overdoped LCCO film (Fig. 7), suggesting that these features are controlled by the doping level of LCCO.

For comparison we have measured the temperature dependence of the magnetic susceptibility and phonon frequencies of the two commercial  $\text{Cu}_2\text{O}$  powders. Although pure  $\text{Cu}_2\text{O}$  is nonmagnetic,[28] the susceptibilities of both powders exhibit pronounced low-temperature Curie tails due to magnetic impurities (Fig. 8). The susceptibility of one of the two samples even exhibits a small

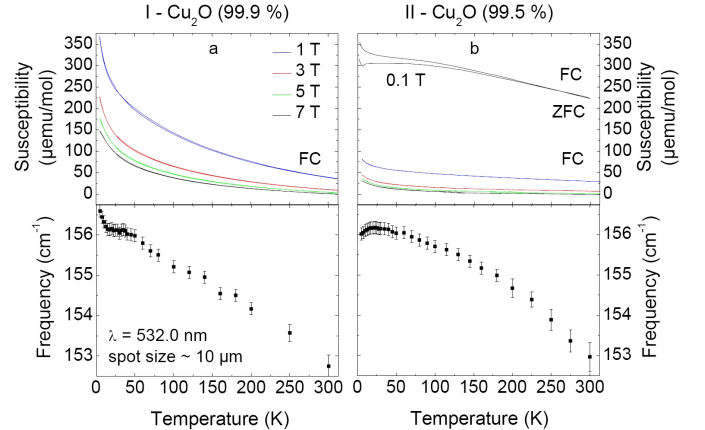


FIG. 8: Temperature dependence of the magnetic susceptibility for different magnetic fields (FC = field cooled, ZFC = zero field cooled), and frequency of the  $\Gamma_{15}^{(1)}$  mode of two compressed  $\text{Cu}_2\text{O}$  powder samples with different purity levels.

anomaly at low magnetic fields and  $T \sim 6$  K, and some field hysteresis over a wider temperature range (Fig. 8b). These observations agree qualitatively with the recent report of a substantial influence of cation vacancies and small amounts of magnetic impurities on the magnetic properties of  $\text{Cu}_2\text{O}$ . [29] The overall temperature dependence of the frequency of the intense  $\Gamma_{15}^{(1)}$  mode shown in Fig. 8 is consistent with the one expected for anharmonic decay. In powder sample I, however, the mode abruptly hardens by  $\sim 0.5 \text{ cm}^{-1}$  between  $T \sim 15$  K and the base temperature of 5 K (Fig. 8a), while powder sample II shows a small hint of a softening (Fig. 8b). These phonon anomalies are surprising, because low-temperature structural instabilities have not been re-

ported for  $\text{Cu}_2\text{O}$ . [30] Moreover, they are apparently uncorrelated with features in the magnetic susceptibility. The phonon anomaly therefore likely arises from sample-specific defects or impurities. Note that the anomaly of the  $\text{Cu}_2\text{O}$  vibration in powder sample I with higher purity level is smaller in magnitude and of opposite sign than the one exhibited by mode A in the underdoped LCCO film (which was fabricated from ultrapure metal sources and is therefore much less affected by magnetic impurities than the commercial powders), and that it occurs at a lower temperature. Nonetheless, the Raman data on  $\text{Cu}_2\text{O}$  do indicate that the low-temperature behavior of the  $\Gamma_{15}^{(1)}$  mode is quite sensitive to microstructural details. This may provide clues to the origin of the anomalous low-temperature behavior of mode A in the LCCO film, which we had identified with the  $\Gamma_{15}^{(1)}$  mode of the  $\text{Cu}_2\text{O}$  inclusions.

In summary, all of the Raman-active phonons observed in the underdoped LCCO film (including modes B and C that are likely due to the LCCO host material as well as mode A, which likely arises from  $\text{Cu}_2\text{O}$  inclusions) exhibit anomalies in their temperature dependence that are reproducible and clearly outside the experimental error bars at a temperature that is consistent with  $T_c$ . In discussing these observations, we first ignore the  $\text{Cu}_2\text{O}$  inclusions and consider the standard picture of superconductivity-induced phonon anomalies which has been established based on Raman data on hole-doped high-temperature superconductors. [11, 31, 32] According to this theory, optical phonons with energies higher than twice the superconducting gap,  $2\Delta$ , harden below  $T_c$ , and their linewidths increase due to an enhanced density of states above the gap. Conversely, phonons with energies below  $2\Delta$  are expected to soften. Deviations from this behavior are predicted only close to  $2\Delta$ . [31] A microscopic formulation of this theory yields a quantitative description of electronic Raman scattering and superconductivity-induced phonon self-energy anomalies in hole-doped  $\text{YBa}_2\text{Cu}_3\text{O}_{6+y}$ . [12] The superconducting energy gap LCCO is known from prior transport measurements on the same films that we have investigated by Raman light scattering. [15] Tunneling characteristics (one of which is reproduced in the inset of Fig. 5) show coherence peaks at an energy of 9 meV, which implies  $2\Delta \sim 75 \text{ cm}^{-1}$ . Since the energies of all of the Raman-active phonons we have discussed are far above  $75 \text{ cm}^{-1}$ , the standard model predicts a weak hardening and broadening below  $T_c$ , in complete contrast to our observations.

Since the standard theory of superconductivity-induced phonon renormalization fails to account for the observations displayed in Fig. 6, we are forced to consider more unconventional scenarios. A possible explanation of the softening and narrowing of the optical modes below  $T_c$  would be a second gap with magnitude in excess of  $2\Delta^* \sim 100 \text{ meV}$  that opens at a temperature close to  $T_c$  or is at least affected by the superconducting phase transition. In this case, all of the Raman-active optical modes would be located below this threshold en-

ergy, and the observed softening could be explained by a straightforward application of the theory of phonon self-energy to this high-energy gap. The narrowing of the phonon linewidths would then be a direct consequence of the reduced number of relaxation channels due to the loss of spectral weight below  $2\Delta^*$ . Angle-resolved photoemission spectroscopy [33, 34] and optical spectroscopy [35, 36] experiments on underdoped NCCO have indeed yielded evidence of a high-energy “pseudogap” that opens up below a temperature  $T^* > T_c$ . Both  $T^*$  and the magnitude of  $\Delta^*$  were found to decrease with increasing doping level, [34, 37], so that  $T^*$  cuts the superconducting phase boundary at optimal doping. [36] In the superconducting regime of NCCO,  $\Delta^* \sim 100 \text{ meV} \gg \Delta$ . [34] Although no evidence has yet been reported of a similar phenomenon in LCCO, it is thus conceivable that interplay between superconductivity and the pseudogap (which may in turn be related to the presence of antiferromagnetic order [34]) could explain the unusual superconductivity-induced phonon self-energy anomalies we have observed. However, nearly identical anomalies exhibited by mode A (which, as we have argued, probably originates in the  $\text{Cu}_2\text{O}$  inclusions) point to a more complex picture in which proximity and/or inverse proximity effects at the LCCO/ $\text{Cu}_2\text{O}$  interface are also involved. It is possible, for instance, that charge transfer across the interface leads to the formation of magnetic  $\text{Cu}^{2+}$  ions and induces cooperative magnetism at the boundaries of the  $\text{Cu}_2\text{O}$  inclusions, which in turn enhances antiferromagnetic order and the pseudogap in LCCO. An investigation of phonon anomalies close the interface by Raman spectroscopy with spatial resolution comparable to the superconducting coherence length is well beyond our current experimental capabilities, but may become possible in the future based on advances in near-field optics. Based on our observations, it appears worthwhile to study such effects systematically using other experimental methods.

In addition to its scientific interest, the technical aspects of our study are of general relevance for the investigation of electron-doped high-temperature superconductors. Inclusions of impurity phases such as lanthanide oxides [1, 2] and  $\text{Cu}_2\text{O}$  are hard to avoid during synthesis and continue to be present in state-of-the-art crystals and films. They are also difficult to detect based on standard x-ray diffraction, either because epitaxial intergrowth leads to Bragg peak positions that are similar to those of the host phase [1, 2] or because powder averaging greatly reduces the intensity of the impurity Bragg reflections. Note, in particular, that the  $\text{Cu}_2\text{O}$  inclusions in our LCCO films required an experimental setup with a ratio of LCCO Bragg intensities to the noise floor of  $\sim 10^4$  (Fig. 2), which goes beyond the typical diagnostics run on thin films. We have shown that both electron microscopy and micro-Raman spectroscopy are powerful, complementary diagnostic tools (Fig. 4). As we have seen, a thorough understanding of impurity inclusions is important not only for transport, but also for spectro-

scopic measurements.

We thank Y. Kuru, B. Bohnenbuck, C. Busch, M. Konuma, E. Brücher, M. Schaloske, R.K. Kremer, and A. Schulz for experimental support, and M. Cardona, D.

Manske, and R. Zeyher for fruitful discussions. This work was supported by the Deutsche Forschungsgemeinschaft (DFG) through project K1930/11.

- 
- [1] P.K. Mang, S. Laroche, A. Mehta, O.P. Vajk, A.S. Erickson, L. Lu, W.J.L. Buyers, A.F. Marshall, K. Prokes, and M. Greven, *Phys. Rev. B* **70**, 094507 (2004)
- [2] G. Roberge, S. Charpentier, S. Godin-Proulx, P. Rauwel, K.D. Truong, P. Fournier, *J. Cryst. Growth* **311**, 1340 (2009)
- [3] For a review, see N.P. Armitage, P. Fournier, and R.L. Greene, preprint arXiv:0906.2931
- [4] M. Naito and M. Hepp, *Jpn. J. Appl. Phys.* **39**, L485 (2000)
- [5] A. Sawa, M. Kawasaki, H. Takagi, Y. Tokura, *Phys. Rev. B* **66**, 014531 (2002)
- [6] Y. Krockenberger, J. Kurian, A. Winkler, A. Tsukada, M. Naito, and L. Alff, *Phys. Rev. B* **77**, 060505(R) (2008)
- [7] M. Naito, A. Tsukada, T. Greibe, and H. Sato, *Proc. SPIE* **4811**, 140 (2002)
- [8] A. Tsukada, H. Yamamoto, and M. Naito, *Phys. Rev. B* **74**, 174515 (2006)
- [9] A. Tsukada, Y. Krockenberger, M. Noda, H. Yamamoto, D. Manske, L. Alff, and M. Naito, *Solid State Commun.* **133**, 427 (2005)
- [10] For a review, see T.P. Devereaux and R. Hackl, *Rev. Mod. Phys.* **79**, 175 (2007)
- [11] C. Thomsen, in *Light Scattering in Solids VI, Topics Appl. Phys.*, edited by M. Cardona and G. Güntherodt (Springer, 1991), Vol. 68, p. 285
- [12] M. Bakr, A.P. Schnyder, L. Klam, D. Manske, C.T. Lin, B. Keimer, M. Cardona, and C. Ulrich, *Phys. Rev. B* **80**, 064505 (2009)
- [13] G. Blumberg, A. Koitzsch, A. Gozar, B.S. Dennis, C.A. Kendziora, P. Fournier, and R.L. Greene, *Phys. Rev. Lett.* **88**, 107002 (2002)
- [14] M.M. Qazilbash, A. Koitzsch, B.S. Dennis, A. Gozar, Hamza Balci, C.A. Kendziora, R.L. Greene, and G. Blumberg, *Phys. Rev. B* **72**, 214510 (2005)
- [15] M. Wagenknecht, D. Koelle, R. Kleiner, S. Graser, N. Schopohl, B. Chesca, A. Tsukada, S.T.B. Goennenwein, and R. Gross, *Phys. Rev. Lett.* **100**, 227001 (2008); M. Wagenknecht, M. Rahlenbeck, D. Koelle, R. Kleiner, A. Tsukada, S.T.B. Goennenwein, and R. Gross, submitted to *Phys. Rev. B*; M. Rahlenbeck, unpublished data
- [16] M. Wagenknecht, *Korngrenz-Tunnelspektroskopie am elektronendotierten Kupratsupraleiter  $La_{2-x}Ce_xCuO_4$* , Ph.D. thesis, Tübingen University, 2008
- [17] T. Greibe, *MBE growth of superconducting thin films*, Technical report, NTT Basic Research Laboratories, 2001
- [18] V.G. Hadjiev, I.Z. Kostadinov, L. Bozukov, E. Dinolova, and D.M. Mateev, *Solid State Commun.* **71**, 1093 (1989)
- [19] S. Sugai, T. Kobayashi, and J. Akimitsu, *Phys. Rev. B* **40**, 2686 (1989)
- [20] E.T. Heyen, R. Liu, M. Cardona, S. Piñol, R.J. Melville, D. McK. Paul, E. Morán, and M.A. Alario-Franco, *Phys. Rev. B* **43**, 2857 (1991)
- [21] Y. Petroff, P.Y. Yu, and Y.R. Shen, *Phys. Rev. B* **12**, 2488 (1975)
- [22] Y. Petroff, P.Y. Yu, and Y.R. Shen, *Phys. Rev. Lett.* **29**, 1558 (1972)
- [23] K. Huang, *Z. Phys.* **171**, 213 (1963)
- [24] Y. Petroff, *J. Phys. (Paris) Colloq. C3*, **35**, 277 (1974)
- [25] P.Y. Yu, Y.R. Shen, and Y. Petroff, *Solid State Commun.* **12**, 973 (1973)
- [26] J. Menéndez and M. Cardona, *Phys. Rev. B* **29**, 2051 (1984)
- [27] V.G. Hadjiev, X. Zhou, T. Strohm, and M. Cardona, *Phys. Rev. B* **58**, 1043 (1998)
- [28] H.L. Schlafer and G. Gliemann, *Basic principles of Ligand Field Theory* (Wiley, New York 1969) p. 120
- [29] Ch. Chen, L. He, L. Lai, H. Zhang, J. Lu, L. Guo, and Y. Li, *J. Phys.: Condens. Matter* **21**, 145601 (2009)
- [30] A. Werner and H. D. Hochheimer, *Phys. Rev. B* **25**, 5929 (1982)
- [31] R. Zeyher and G. Zwicknagl, *Z. Phys. B - Condensed Matter* **78**, 175 (1990)
- [32] T.P. Devereaux, *Phys. Rev. B* **50**, 10287 (1994)
- [33] N.P. Armitage, D.H. Lu, C. Kim, A. Damascelli, K.M. Shen, F. Ronning, D.L. Feng, P. Bogdanov, and Z.-X. Shen, *Phys. Rev. Lett.* **87**, 147003 (2001)
- [34] H. Matsui, T. Takahashi, T. Sato, K. Terashima, H. Ding, T. Uefuji, and K. Yamada, *Phys. Rev. B* **75**, 224514 (2007)
- [35] Y. Onose, Y. Taguchi, K. Ishizaka, and Y. Tokura, *Phys. Rev. Lett.* **87**, 217001 (2001)
- [36] A. Zimmers, J.M. Tomczak, R.P.S.M. Lobo, N. Bonetemp, C.P. Hill, M.C. Barr, Y. Dagan, R.L. Greene, A.J. Millis, and C.C. Homes, *Europhys. Lett.* **70**, 225 (2005)
- [37] Y. Dagan, M.M. Qazilbash, and R.L. Greene, *Phys. Rev. Lett.* **94**, 187003 (2005)